Elastic Scattering of 17-Mev Protons by Nuclei*

I. E. Dayton† and G. Schrank
Palmer Physical Laboratory, Princeton University, Princeton, New Jersey
(Received July 13, 1955)

The absolute differential cross section for the elastic scattering of 17.00±0.05 Mev (center of mass energy) protons has been measured for twelve elements: Be, C, Al, Fe, Co, Ni, Cu, Zn, Rh, Ag, Pt, and Au. Between 31 and 39 angles were taken for each element with a five-degree (or less) interval ranging from 15 to 172 degrees. The estimated standard deviation of each point is 2.5%. The scattered protons are detected by a NaI(Tl) crystal whose energy resolution is about 2.5%, with the result that in the majority of cases all inelastically scattered protons are rejected.

I. INTRODUCTION

ALTHOUGH considerable progress has been made in the interpretation of medium-energy nucleon-nucleus elastic scattering data using the optical model, no really satisfactory agreement between theory and experiment has yet been obtained. It has been shown that no square well potential will fit the experimental data,[1,2] while long-tailed potentials appear to improve the agreement considerably.[3] In addition, it is felt that nuclear, and perhaps electromagnetic, spin-orbit forces might influence the shape of the angular distributions at these energies. In order to examine these effects, machine calculations based on a multiparameter optical model are in progress here and elsewhere.[4]

The inauguration of these calculational programs provided the incentive for extending and refining the experiment on proton elastic scattering begun by Dayton.[1] Although the general method is the same, many refinements in experimental design and technique have been introduced to improve the accuracy and reliability of the data. The twelve target elements have been chosen to cover a wide range in atomic number and also provide sets of neighboring elements to facilitate the detection of possible effects due to nuclear spin, shape, and shell structure.

II. DESIGN OF EXPERIMENT

The experimental arrangement is shown schematically in Fig. 1. The proton beam is deflected electrostatically from the Princeton FM cyclotron and focused in the horizontal and vertical directions by two pairs of wedge-shaped magnets. Before reaching the target the beam passes through two $\frac{1}{4}$-in. diameter apertures, the first 1.32 meters from the target and the second 0.56 meter from the target. Each of these collimators is followed by baffles to remove slit-scattered protons from the beam. The beam spot in the center of the chamber was roughly $\frac{3}{8}$-in. in diameter. The detector solid angle was determined by the fixed $\frac{3}{16}$-in. diameter aperture in front of the counter and by the distance of the counter from the center of the scattering chamber, which was varied from 20 to 50 cm. The pulse-height distribution from the detector was recorded on a 20-channel pulse-height analyzer.

It was anticipated at the outset that a great deal of experimental data would be necessary to observe all the details in the angular distributions for a dozen elements. In actual fact, about 600 runs were made with the twenty-channel analyzer and about two million counts were recorded for the final data. In order to minimize counting times without introducing large corrections, experimental and mathematical investigations were made of the effects due to finite geometry, multiple scattering, and counting rate.

Geometry and Multiple Scattering

Where the slope and curvature of the cross section *vs* angle curve are large, the observed cross section may be significantly different from the value at a point because of effects resulting from finite geometry and multiple scattering in the target. In order to eliminate effects due to finite geometry a general correction expression for a parallel incident beam filament was obtained. The details of the derivation are given in the appendix. The result is given in the usual form of an expansion:

$$Y=Y_0\left[A+B\frac{\sigma'(\theta_0)}{\sigma(\theta_0)}+C\frac{\sigma''(\theta_0)}{\sigma(\theta_0)}\right],$$

where A, B, and C are functions of the geometry.

For multiple-scattering corrections, a similar expansion due to Chase and Cox[5] was used.

$$Y=Y_0\left[1+\tfrac{1}{4}\epsilon^2\left(\frac{\sigma'(\theta_0)}{\sigma(\theta_0)}\cot\theta_0+\frac{\sigma''(\theta_0)}{\sigma(\theta_0)}\right)\right].$$

In this expression ϵ is the rms value of the multiple-scattering distribution taken from the theory of Williams.

* This work was supported by the U. S. Atomic Energy Commission and the Higgins Scientific Trust Fund.
† Now at the Atomic Energy Division, The Babcock and Wilcox Company, Lynchburg, Virginia.
[1] I. E. Dayton, Phys. Rev. **95**, 754 (1954).
[2] D. M. Chase and F. Rohrlich, Phys. Rev. **94**, 81 (1954).
[3] R. D. Woods and D. S. Saxon, Phys. Rev. **95**, 577 (1954).
[4] Aron, McIntosh, Schrank and Bigelow, Phys. Bull. **99**, 629(A) (1955).
[5] C. T. Chase and R. T. Cox, Phys. Rev. **58**, 246 (1940).

Experimental tests of these relations gave good agreement with the geometrical correction expression and acceptable agreement with the multiple scattering relation. The experimental parameters were chosen so that the corrections never exceeded 3% for geometrical effects and 1.5% for multiple scattering.

Counting Rate

The use of a pulsed accelerator such as an FM cyclotron introduces special problems with regard to counting rates. The Princeton cyclotron has a repetition rate of 2000 pulses per second and each pulse is about 20 microseconds long. The twenty-channel analyzer has a dead time of 20 microseconds in each of the regular channels, which means that not more than one count per channel per beam pulse can be recorded. By using simple probability theory it is possible to compute the maximum allowable counting rate in a channel for a given percentage loss due to dead time. This calculation checked nicely with a measurement of observed cross section as a function of counting rate. The counting rate was kept low enough so that the loss due to dead time was 0.2% or less and hence negligible.

III. APPARATUS

Scattering Chamber

The experiment was carried out in the Princeton 60-in. precision scattering chamber. This chamber has been described in detail by Yntema and White[6] and only the salient features will be mentioned here. The target holder enters the chamber through an air lock in the center of the lid so that targets can be changed without disturbing the chamber vacuum. The target is automatically positioned at the exact center of the scattering table. The over-all chamber alignment and table accuracy is such that the scattering angle can easily be read to the nearest 0.1 degree.

Detector

The scattered protons were detected by a single NaI(Tl) crystal mounted on the face of a Du Mont 6291 photomultiplier tube. The crystal, which was cleaved from a larger block, was about 0.5 inch square and slightly thicker than the range of the protons. With the layout and shielding of the experimental area, the neutron and γ-ray background is completely negligible with this type of detector for elastic scattering experiments at this energy. The photomultiplier high voltage was supplied by a highly regulated (0.01%) electronic circuit. After passing through a preamplifier and cathode follower, the pulses were sent into an Atomic Instrument Company Model 520 Twenty-Channel Pulse-Height Analyzer. Gain and channel width were adjusted so that the upper 15% to 20% of the pulse-height distribution was recorded. The

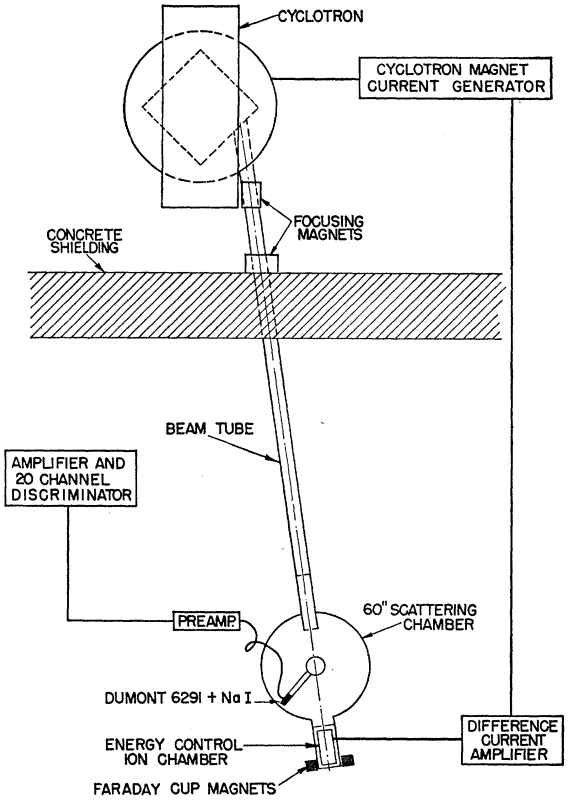

FIG. 1. Schematic drawing of the experimental setup.

over-all energy resolution of the detection system was about 2.5%. The angular resolution varied from one-half to two degrees depending upon angle and solid angle.

As will be discussed later, this energy resolution was sufficient to rule out errors due to the inclusion of inelastically scattered protons for all elements up to Zn. This energy resolution also eliminated effects due to slit scattering from the detector collimator because any proton whose total path length in the brass collimator was more than about 0.0008 in. would be rejected. Calculations by Courant[7] bear out the conclusion that the increase in effective solid angle in this case is negligible.

The stability of the detection system was excellent. For identical operating conditions, the output pulse height as recorded varied less than 1% from day to day.

Beam Current

At the back end of the scattering chamber the beam passes through a 0.002-in. Dural foil and then is collected in a Faraday cup. The region surrounding the Faraday cup is maintained at a high vacuum (about 10^{-5} mm Hg) with a diffusion pump in order to reduce effects due to secondary electrons. The Faraday cup is also equipped with a large suppressor magnet. Previous

[6] J. L. Yntema and M. G. White, Phys. Rev. **95**, 1226 (1954).

[7] E. D. Courant, Rev. Sci. Instr. **22**, 1003 (1951).

measurements[6] have shown that secondary-electron effects are small enough to be neglected.

The beam collected in the cup charges up one or more polystyrene capacitors in parallel and the voltage across these is measured with a quadrant electrometer. The electrometer was calibrated every few hours with a precision potentiometer. It was found that during a day's run the calibration of the electrometer remained constant to about 0.1%, the smallest change which could be detected. Over a period of four months the calibration slowly changed by about 0.5%. The capacitors, the same ones used by Yntema and White[6] and by Brockman,[8] had been calibrated at the National Bureau of Standards with a probable error of 0.5%. During operation the Faraday cup was never more than one volt away from ground potential. Practically, this meant that at some angles, it was necessary to charge and discharge the capacitors more than once to obtain enough counts. Yntema and White[6] have shown that this cup can be operated at least six volts away from ground potential with no detectable change in efficiency. The leakage of the entire circuit was shown to be negligible by charging it up and leaving it for several hours. This system of beam current measurement, while not as convenient as numerous electronic devices designed for the purpose, had the distinct advantage of being very stable and completely reliable. The assignment of an over-all uncertainty of 1% in the measurement of the beam current seems reasonable.

Beam Energy

In the experiment previously reported,[1] obtaining the same cyclotron beam energy on different days proved to be one of the major experimental difficulties. Similar troubles have been reported by other workers. In order to eliminate this difficulty and to provide a continuous monitor on the beam energy, a beam energy control circuit was designed and constructed.[9]

Protons elastically scattered from the target through about seven degrees in the vertical direction leave the scattering chamber through a small aperture and enter an argon-filled, parallel-plate ionization chamber. Most of their range is spent in aluminum absorbers placed in front of this ion chamber so that the end of their range is in the ion chamber. By means of a double-electrode arrangement which determines the position of the peak of the Bragg curve, the mean energy of the beam is determined, and by feeding the difference signal from these electrodes back into the cyclotron magnet current control, the beam energy is stabilized. With this arrangement the mean energy was stabilized to 0.1% and measured to 0.3%. Different beam energies can be selected by changing the aluminum absorber thickness in front of the ion chamber.

The aluminum equivalent of all the material through which the beam passes is calculated using results of Aron, Hoffman and Williams,[10] and a correction is applied for the distance between the peak of the Bragg curve and the mean range of the protons. These results checked to better than 2 mg/cm^2 aluminum with a direct measurement of the integral number-distance curve. The absolute beam energy was then obtained from the range-energy relation of Bichsel and Mozley.[11] In the calibration of the system, correction for the proton's energy loss in scattering was included.

The sensivity of this device increases with increasing atomic number of the target, since small-angle scattering goes as Z^2. With all except the lightest materials used in this experiment, a change in beam energy was more sensitive to the various operating parameters of the cyclotron than had previously been believed. For example, a change in deflector voltage of 1.5 kv out of 50 kv changed the mean energy of the external beam by about 100 kev. Changes in the focusing magnet currents which occurred during normal operation could produce beam energy changes of a hundred kev or more. A number of hysteresis effects were noted: changing some controls and then returning them to their original value did not return the beam energy to its original value.

Because of the ease with which the beam energy could now be measured and changed, it was decided to perform the experiment at a mean energy of 17.00

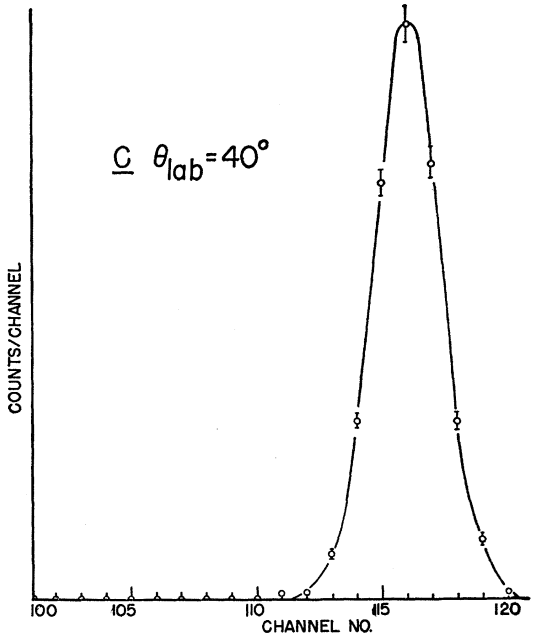

FIG. 2. Pulse-height distribution showing the energy resolution and low background obtained in the absence of inelastic scattering.

[8] K. W. Brockman, Princeton University thesis, 1954 (unpublished).
[9] G. Schrank, Rev. Sci. Instr. **26**, 677 (1955).
[10] Aron, Hoffman, and Williams, Atomic Energy Commission Report AECU-663 (unpublished).
[11] H. Bichsel and R. F. Mozley, Phys. Rev. **94**, 764 (1954).

Mev in the center-of-mass system of each element. This energy was held within ± 50 kev except in the case of Be where the error in the energy was ± 100 kev because of the decreased sensitivity of the control for low-Z materials. The proton energy distribution in the beam had a full width at half-maximum of about 250 kev.

Targets

In a survey experiment of this kind, it is convenient to choose the particular elements to be investigated to minimize the experimental difficulties. Consequently, wherever possible, those elements were chosen which have no levels below about 0.5 Mev, since this is about the minimum peak separation that can be handled conveniently with the existing resolution. (This criterion was not met by all the heavy elements and other considerations had to be employed.) Only those elements which could be put into foil form were considered since the existing precision scattering apparatus was already set up for foil scattering. Fewer corrections are involved with foil targets compared to gas targets and the experiment is, on the whole, somewhat neater.

With a few exceptions, the target foils were obtained from commercial sources. These foils are believed to be quite uniform for two reasons. When several targets of the same size were cut out of the same piece of material, they all weighed within 1% of each other, thus indicating no thickness variations over large distances. In those foils which had pinholes, the pinholes showed a uniform distribution. The spacing of the pinholes was very small compared to the dimensions of the beam spot.

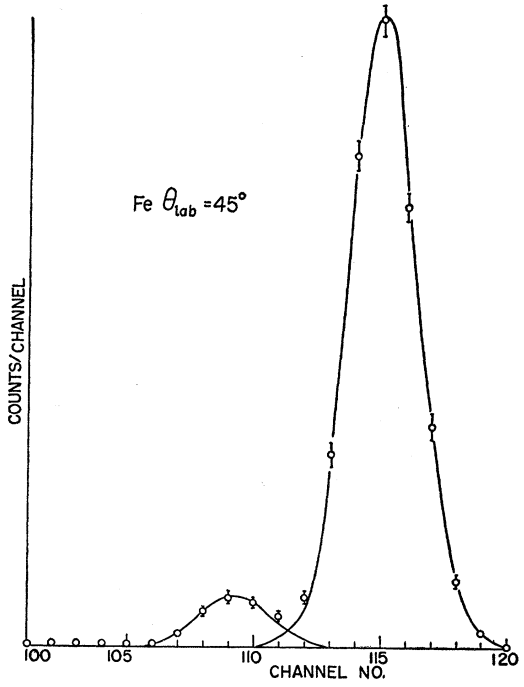

FIG. 3. Pulse-height distribution from scattering from Fe in the forward direction. The small peak is inelastic scattering to the 0.82-Mev level.

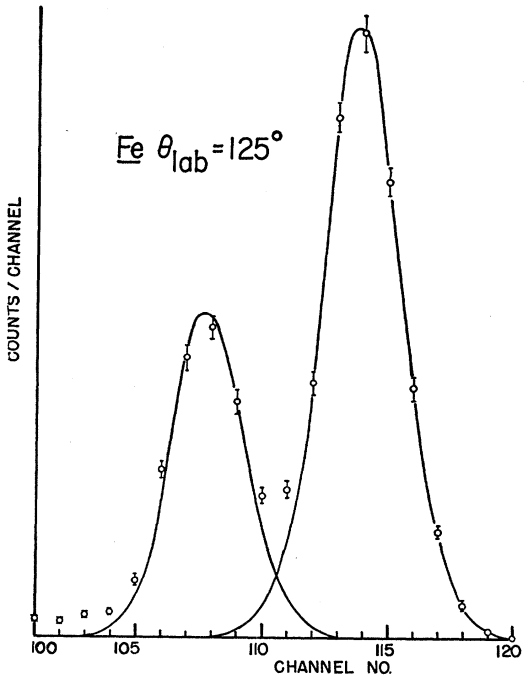

FIG. 4. Pulse-height distribution obtained at the second minimum in the Fe cross section. The second peak is inelastic scattering to the 0.82-Mev level.

The carbon target was in the form of polystyrene. The uniformity of this material can be checked very easily by observing interference fringes. Polystyrene is much more uniform than polyethylene and does not wrinkle with use. All that can be said about the 0.002-in. Be foil (of which only one was available), is that micrometer measurements showed no variations in thickness.

The Co and Zn foils were prepared by electroplating from an aqueous solution on to a polished piece of stainless steel. After a sufficient thickness of material had been deposited, it was easily peeled off the backing and formed a self-supporting foil. Large parallel electrodes were used in an effort to obtain uniform deposition.[12]

In three cases, elastic scattering peaks due to impurities in the target were observed. These peaks can easily be distinguished from peaks due to inelastic scattering in the target material because of the difference in center-of-mass motion of the two materials. Peaks due to impurities were observed in the Be, Co, and Zn targets, and by measuring the change in pulse height with scattering angle the impurities were all identified as oxygen. At scattering angles greater than 55 degrees the impurity peak was clearly resolved from the main

[12] We are indebted to Mr. J. D. Voorhies and Dr. R. A. Naumann for developing this technique and for producing an ample supply of foils.

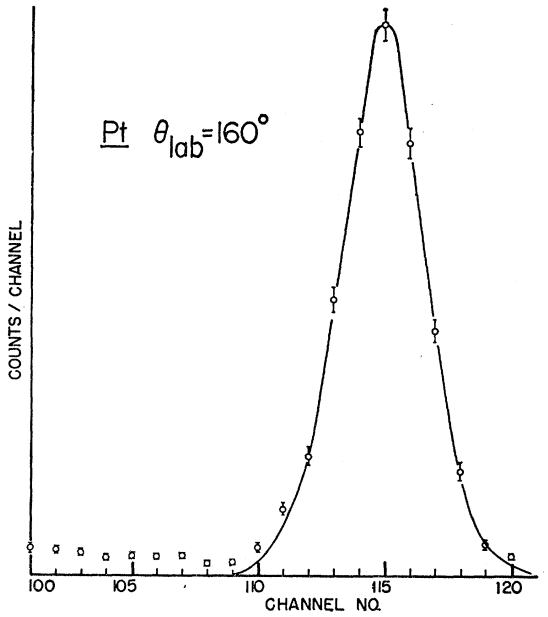

FIG. 5. Pulse height distribution from scattering from Pt in the backward direction.

elastic scattering peak, and hence the only correction required was for the weight of oxygen in the foil. At angles less than 55 degrees it was necessary to subtract the contribution of the impurity from the combined elastic peak. This was done by measuring the angular distribution of elastic scattering from an air target, fitting the oxygen distribution to angles greater than 55 degrees, and then subtracting the oxygen contribution for angles less than 55 degrees.[13] By making use of these data it was also possible to obtain quite accurately the amount of oxygen contamination in each of the foils.

The situation regarding foil contamination and inelastic scattering in each target material is summarized as follows:

Be: Oxygen contamination 4.6% by weight, maximum subtraction at low angles correction 4.0%. Lowest O^{16} level at 6.06 Mev does not overlap the Be elastic peak at any angle. Lowest Be level completely resolved from elastic peak.

C: Peak due to H in polystyrene foil clearly resolved from C at all angles. C inelastic peaks clearly resolved. Figure 2 shows a typical pulse-height distribution obtained from this target and illustrates both the energy resolution and the low background that were obtained.

Al: Elastic peak clearly resolved from lowest level at 0.84 Mev.

Fe: Elastic peak clearly separated from peak of lowest (0.82 Mev) level in Fe^{56} (92% abundance). First level of Fe^{54} (5.8% abundance) is probably 1.5 Mev and would be clearly separated. The first few levels in Fe^{57} (2.2% abundance) are at 0.014 and 0.131 Mev and would be included in the elastic peak. At minima in the differential cross section these inelastic levels would make the observed elastic scattering at most 1% too high. Figure 3 shows a pulse-height distribution obtained from scattering in the forward direction, and Fig. 4 shows a distribution obtained at the second minimum in the differential cross section. These pulse-height distributions are typical of those obtained for Al and the group of elements from Fe to Zn. In the case of Fe it was possible to obtain the angular distribution of the inelastic scattering from the 0.82-Mev level, and this has been reported elsewhere.[14]

Co: Oxygen contamination 2.7% by weight. Lowest level at 1.1 Mev clearly separated.

Ni: Five stable isotopes, but all known levels are higher than 0.65 Mev and hence should be clearly separated. Considerable inelastic scattering was observed around 1.3 Mev, but nothing below that. The shape of the elastic peak indicated no appreciable inelastic problem at any angle.

Cu: Lowest level in either stable isotope is at about 1.0 Mev.

Zn: Oxygen contamination 2.5% by weight. Zn has five stable isotopes and in all but one of these the lowest level appears to be higher than one Mev. Zn^{67} (4.1% abundance) has a number of low-lying states (0.09, 0.182, 0.39, ···Mev). On the basis of reasonable estimates of the excitation of these states, it is possible

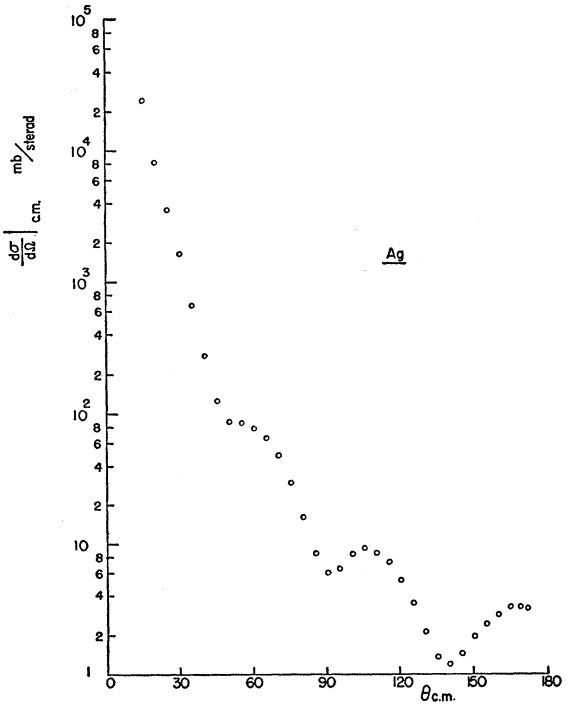

FIG. 6. Plot showing the individual points measured for Ag. The estimated standard deviation is given by the size of the points.

[13] We wish to thank Dr. K. W. Brockman for the use of his gas scattering apparatus and for his assistance in making these measurements.

[14] Schrank, Gugelot, and Dayton, Phys. Rev. **96**, 1156 (1954).

TABLE I. Experimental results transformed to the center-of-mass system. The angles are in degrees and the cross sections in mb/sterad.

$\theta_{c.m.}$	$\frac{d\sigma}{d\omega}\Big\|_{c.m.}$
Be	
16.8	704.
22.3	536.
27.8	379.
33.3	267.
38.8	168.
44.2	94.8
49.6	50.3
55.0	24.3
60.4	11.8
65.7	7.26
68.8	6.69
70.9	6.83
76.1	7.78
81.3	9.05
86.4	9.64
91.5	10.5
96.5	10.1
101.5	9.16
106.4	8.22
112.3	6.82
117.1	5.93
121.9	5.07
126.6	4.18
131.3	3.44
135.9	2.82
140.5	2.40
145.1	2.08
149.7	1.84
154.2	1.79
158.7	1.77
163.2	1.91
168.5	2.10
173.9	2.17
C	
16.4	726.
21.8	557.
27.1	409.
32.5	289.
37.9	184.
43.2	115.
48.5	64.0
53.8	35.8
59.0	20.9
64.3	16.2
69.5	15.7
74.6	16.4
79.8	19.8
84.8	21.8
89.9	24.0
94.9	23.7
99.9	24.1
104.8	23.0
109.7	20.3
114.6	17.6
119.5	14.5
124.3	11.1
129.0	7.72
133.8	4.87
138.5	3.12
141.3	2.66
143.2	2.60
145.1	2.59
147.9	3.31
150.6	4.34
152.5	5.16
157.1	7.92
161.7	10.9
167.3	14.6
172.8	16.8

$\theta_{c.m.}$	$\frac{d\sigma}{d\omega}\Big\|_{c.m.}$
Al	
15.7	1850.
20.8	860.
26.0	426.
31.2	187.
34.3	99.6
36.3	59.3
39.4	24.0
41.5	11.7
43.5	6.79
44.6	6.08
45.6	7.13
46.6	8.99
48.7	14.2
51.7	24.5
56.9	38.9
62.0	45.6
67.0	45.0
72.1	34.9
77.2	25.4
82.2	16.4
87.2	10.3
92.2	7.48
97.2	6.32
102.2	6.38
107.2	6.76
112.1	7.40
117.0	7.51
122.0	7.69
126.9	8.44
131.7	7.98
136.6	7.16
141.5	6.72
146.3	5.89
151.2	5.17
156.0	4.63
160.8	4.12
166.6	4.13
172.4	4.24
Fe	
15.4	5410.
20.5	1760.
25.5	767.
30.6	376.
35.7	215.
40.8	140.
45.8	111.
50.9	79.9
55.9	50.7
61.0	25.7
66.0	9.17
69.1	4.50
71.1	3.53
73.1	3.95
76.1	5.89
81.1	10.5
86.1	14.8
91.1	15.2
96.1	13.1
101.1	10.1
106.1	6.44
111.1	3.94
116.0	2.19
121.0	1.75
125.9	2.00
130.9	2.58
135.8	3.31
140.8	4.00
145.7	4.43
150.6	4.67

$\theta_{c.m.}$	$\frac{d\sigma}{d\omega}\Big\|_{c.m.}$
Fe	
155.5	4.61
160.5	4.21
166.3	3.39
172.2	2.61
Co	
15.4	5330.
20.4	1780.
25.5	797.
30.6	392.
35.7	222.
40.7	132.
45.8	96.8
50.9	67.0
55.9	41.3
61.0	19.0
64.0	10.6
66.0	7.35
69.0	4.82
70.0	4.82
71.0	4.96
73.0	5.81
76.1	8.31
81.1	13.0
86.1	15.3
91.1	14.6
96.1	12.0
101.1	8.01
106.1	4.75
111.0	2.83
116.0	1.96
121.0	2.11
125.9	2.50
130.9	3.30
135.8	3.69
140.7	3.97
145.7	4.07
150.6	4.20
155.5	4.00
160.4	3.52
165.4	3.00
172.2	2.31
Ni	
15.4	6360.
20.4	1920.
25.5	830.
30.6	422.
35.7	244.
40.7	167.
45.8	119.
50.9	83.4
55.9	48.9
61.0	23.4
64.0	12.4
66.0	7.99
69.0	4.71
71.0	4.30
73.1	4.97
76.1	7.54
81.1	12.2
86.1	15.4
91.1	15.3
96.1	13.5
101.1	9.55
106.1	6.04
111.0	3.48
116.0	2.38
121.0	2.22
125.9	2.54

$\theta_{c.m.}$	$\frac{d\sigma}{d\omega}\Big\|_{c.m.}$
Ni	
130.9	3.14
135.8	3.86
140.7	4.24
145.7	4.73
150.6	5.14
155.5	5.34
160.4	5.15
166.3	4.48
172.2	4.06
Cu	
15.3	6900.
17.4	4170.
20.4	2340.
25.5	1060.
30.5	549.
35.6	300.
40.7	171.
45.7	113.
50.8	69.6
55.8	37.1
60.9	15.4
63.9	8.28
65.9	6.44
67.9	5.92
70.9	7.68
73.0	9.54
76.0	13.7
81.0	18.2
86.0	19.7
91.0	16.9
96.0	11.7
101.0	7.03
106.0	3.48
110.9	1.89
112.9	1.80
115.9	1.94
120.9	2.84
125.8	3.85
130.8	4.47
135.7	4.44
140.7	4.42
145.6	4.27
148.6	4.03
150.5	3.93
154.5	3.79
155.5	3.61
160.4	3.30
166.3	2.79
172.2	2.16
Zn	
15.3	6570.
20.4	2190.
25.5	987.
30.5	496.
35.6	262.
40.7	153.
45.7	93.2
50.8	57.3
55.8	30.5
60.9	13.4
63.9	7.91
65.9	6.61
67.9	6.55
70.9	8.58
76.0	12.6
81.0	16.6
86.0	16.0
91.0	13.4

TABLE I.—(*Continued*).

$\theta_{c.m.}$	$\frac{d\sigma}{d\omega}\Big\|_{c.m.}$	$\theta_{c.m.}$	$\frac{d\sigma}{d\omega}\Big\|_{c.m.}$	$\theta_{c.m.}$	$\frac{d\sigma}{d\omega}\Big\|_{c.m.}$	$\theta_{c.m.}$	$\frac{d\sigma}{d\omega}\Big\|_{c.m.}$
Zn		Rh		Ag		Pt	
96.0	9.98	110.6	7.87	130.5	2.12	150.2	6.85
101.0	5.55	115.6	7.07	135.5	1.35	155.2	6.38
106.0	2.48	120.6	5.73	140.4	1.20	160.2	6.35
110.9	1.37	125.5	4.04	145.4	1.43	166.2	6.45
112.9	1.35	130.5	2.59	150.4	1.94	171.1	6.46
115.9	1.68	135.5	1.72	155.3	2.41		
120.9	2.50	140.4	1.20	160.3	2.84	Au	
125.8	3.41	145.4	1.23	165.2	3.26	25.2	12 700.
130.8	3.91	150.4	1.59	169.2	3.28	30.2	5670.
135.7	3.90	155.3	2.12	172.2	3.19	35.3	2720.
140.7	3.63	160.3	2.80			40.3	1560.
145.6	3.08	166.2	3.22	Pt		45.3	1060.
150.5	2.77	170.2	3.28	20.2	32 000.	50.3	744.
155.5	2.57			25.2	13 400.	55.3	451.
160.4	2.42	Ag		30.2	5770.	60.4	255.
166.3	2.05	15.2	24 300.	35.3	2760.	65.4	141.
172.2	1.77	20.3	8200.	40.3	1520.	67.4	119.
		25.3	3580.	45.3	1030.	70.4	98.9
Rh		30.4	1670.	50.3	718.	75.4	89.6
15.2	23 300.	35.4	667.	55.3	445.	80.4	79.8
20.3	7390.	40.5	277.	60.4	249.	85.4	69.6
25.3	3260.	45.5	124.	65.4	147.	90.4	53.2
30.4	1540.	50.5	86.7	70.4	106.	95.4	37.0
35.4	642.	55.5	84.5	75.4	91.0	100.4	25.7
40.5	264.	60.6	77.0	80.4	84.8	105.4	18.1
45.5	117.	65.6	65.2	85.4	74.3	110.4	15.7
50.5	76.5	70.6	48.1	90.4	54.7	115.4	14.7
55.5	70.0	75.6	29.5	95.4	38.5	120.4	15.0
60.6	70.1	80.6	16.0	100.4	25.7	125.3	14.9
65.6	63.4	85.6	8.40	105.4	18.8	130.3	13.2
70.6	47.5	90.6	5.98	110.4	15.3	135.3	10.4
75.6	32.0	95.6	6.44	115.4	15.4	140.3	8.22
80.6	17.5	100.6	8.31	120.4	15.4	145.3	6.71
85.6	8.79	105.6	9.20	125.3	14.6	150.2	6.01
90.6	5.60	110.6	8.46	130.3	13.0	155.2	5.82
95.6	5.18	115.6	7.23	135.3	11.3	160.2	5.62
100.6	6.23	120.6	5.26	140.3	9.06	166.2	5.99
105.6	7.62	125.5	3.50	145.3	7.89	172.1	6.61

that the elastic points might be 1% high at the minima in the elastic cross section with negligible error elsewhere.

Rh: Energy levels at 0.04, 0.295, 0.357, and 0.49 Mev. The 0.49-Mev level appeared quite strongly and was separated out by pulse-height analysis at all angles. However, this separation is just at the limit of resolution and considerable error might be present at some angles for this element. In particular, at the 95-degree minimum in the elastic cross section an 11% correction is required. It is estimated that the limits of error on this subtraction are 11±5%. At the 145-degree minimum a subtraction of 25±10% was necessary. The error due to subtraction of inelastic scattering to the 0.49-Mev level is negligible for angles less than 80 degrees. The marked presence of the 0.49-Mev level would mask any asymmetry in the elastic peak caused by the 0.295- and 0.357-Mev levels. All three of these levels are included in the elastic peak at all angles.

Ag: Scattering to a level at 0.44±0.03 Mev was observed. At the time this was observed, it had not been previously reported, but since then a level at approximately this energy has been detected in Coulomb excitation experiments.[15] Scattering to this level was observed to be essentially identical with that to the Rh level at the same energy and the same remarks can be made about the errors in the Ag curve as were made for Rh. The Ag level at 0.09 Mev would certainly have been included in the elastic peak, and any asymmetry due to the 0.31-Mev level would have been masked by the higher level.

Pt: There are six stable isotopes with many levels below 0.4 Mev, and any inelastic scattering to these levels is included in the elastic peak. However, these levels are apparently much less strongly excited than similar levels for medium A nuclei, since the elastic peak shows no distortion and there is very little inelastic scattering observed outside the elastic peak. (See Fig. 5.) Since the cross section decreases almost monotonically with increasing angle, the worst possible cases are in the range from 140 degrees to 170 degrees. From the shape of the curve and the lack of appreciable low-energy tail, it is estimated that the elastic curve might be at most 3% too high in this region. Any error

[15] N. P. Heydenburg and G. M. Temmer, Phys. Rev. **95**, 861 (1954).

due to inelastic scattering would be negligible at lower angles.

Au: One stable isotope, but again many levels below 0.4 Mev. The same remarks apply here as were made for Pt.

IV. ERRORS

The cross sections were determined from the area under the elastic scattering peak. It is felt that, with the exception of the few cases discussed above, this area can be determined with an accuracy of 1%.

In general, data were taken for each element at five-degree intervals from 15 degrees to 172 degrees. Additional points were taken near minima in the cross sections so that their shape and location could be better defined. At least 2500 counts were taken at each point. The statistical error in counting, combined with the estimated errors of 1% in beam current measurement and 1% in determining the area under the elastic peak leads to a conservative estimate of a standard deviation of 2.5% for each point. Errors in other parameters were negligible compared to those mentioned above.

The extent to which the measured points define a differential cross-section curve can best be seen by observing Fig. 6, which shows a typical example. The uncertainty in cross section is given approximately by the vertical size of the circles. The uncertainty in angle is, however, only ± 0.1 degree. This uncertainty in angle can be ignored in most cases, but it will produce a definite effect if the differential cross section is very steep. As an example, notice in Table I the data for Pt and Au at small angles. At these angles the cross section is almost entirely Rutherford scattering, and hence the cross sections for Au should be higher than those for Pt at the same angles. However, the measured values show the opposite relation. If the differential cross section is taken as

$$\frac{d\sigma}{d\omega}=\left(\frac{Ze^2}{4E}\right)^2 \csc^4\left(\frac{\theta}{2}\right),$$

then the change in cross section with angle is given by

$$d\left(\frac{d\sigma}{d\omega}\right)=-2\cot\left(\frac{\theta}{2}\right)\cdot\frac{d\sigma}{d\omega}d\theta.$$

Putting numbers into this expression from the Pt and Au curves shows that an error in angle of 0.1 degree is more than enough to explain the apparent discrepancy in small-angle cross sections.

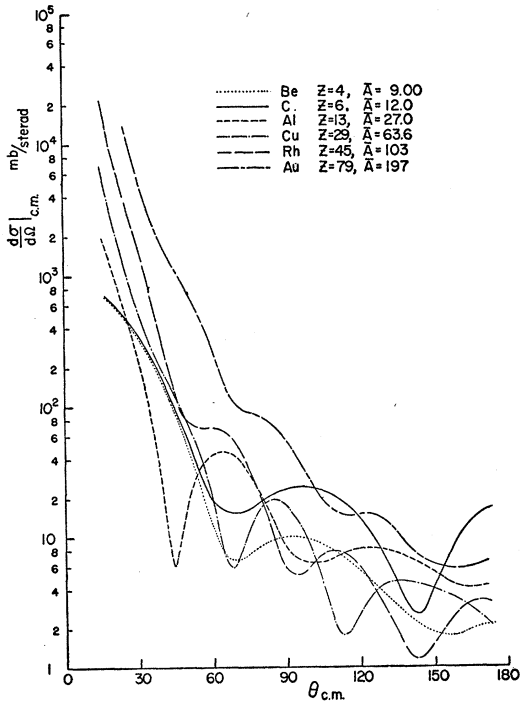

FIG. 7. Measured cross sections in the center-of-mass system for six elements between Be and Au.

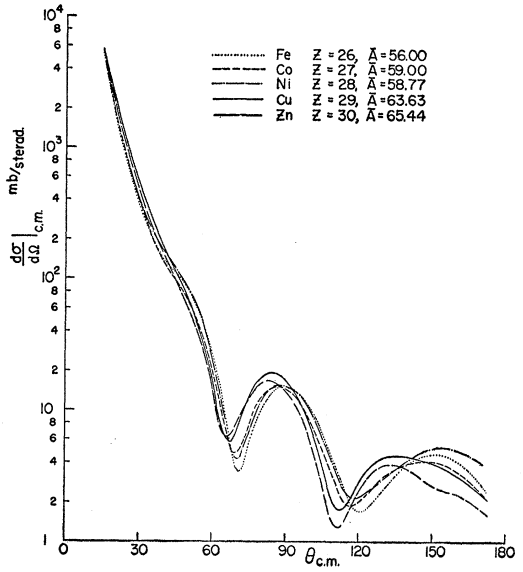

FIG. 8. Measured cross sections in the center-of-mass system for the five elements between Fe and Zn.

V. RESULTS

The results of the experiment, transformed classically to the center-of-mass system, are given in Table I. To exhibit some of the regularities in the data, groups of curves which are smooth fits to the experimental points have been plotted in Figs. 7–10. The changes in differential cross section and ratio R over a range of 6 elements from Be to Au is shown in Figs. 7 and 9.[16] It is immediately apparent that as the size of the nucleus increases, the spacing of the minima in the cross section

[16] The quantity R is the ratio of the measured cross section in the center-of-mass system to the Rutherford scattering cross section, where the Rutherford cross section is taken as $d\sigma/d\omega|_R = (Ze^2/4E_{\text{c.m.}})^2 \csc^4(\theta_{\text{c.m.}}/2)$.

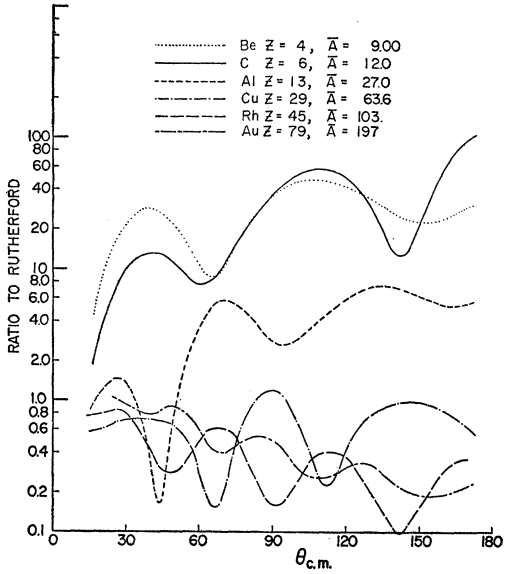

FIG. 9. R (ratio of measured cross section in the center-of-mass system to the Rutherford scattering cross section) for the same six elements as shown in Fig. 7.

decreases. This result, which agrees with what one would expect from the simple picture of a plane wave scattered by a spherical object, is in accord with previous observations. It is of interest to observe that as A increases the average value of R decreases.

Figures 8 and 10 show the variations in cross section and R in the group of five elements from Fe to Zn. Fe, Co, and Ni have almost the same values of $\bar{A}$ and their cross sections have nearly the same shape, although they do differ by almost a factor of two at some points. Cu and Zn have very nearly the same $\bar{A}$ and their curves are also very similar. It is interesting to

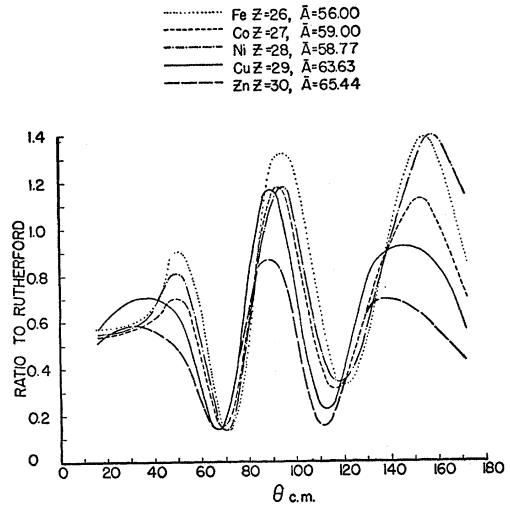

FIG. 10. R (ratio of measured cross section in the center-of-mass system to the Rutherford scattering cross section) for the same five elements as shown in Fig. 9.

notice the kink which occurs at 150 degrees in the Zn cross section. This kink is much like one observed in Cu at the same location and somewhat higher energy (see Figs. 4 and 5 of reference 1).

Figure 11 shows the result of a search for regularities in the location of the minima in the differential cross sections. The location of minima has been plotted as a function of a quantity which is proportional to the reciprocal of the wave number of the incoming particle times the radius of the nucleus. The simple diffraction picture indicates that the position of the forward minima goes at $1/kR$, but this dependence can be justified only for small angles. It is of interest to observe that although the line of lowest slope goes through the origin, the others definitely do not. These three are consistent with an intercept of -28 degrees, but the significance of this is not clear.

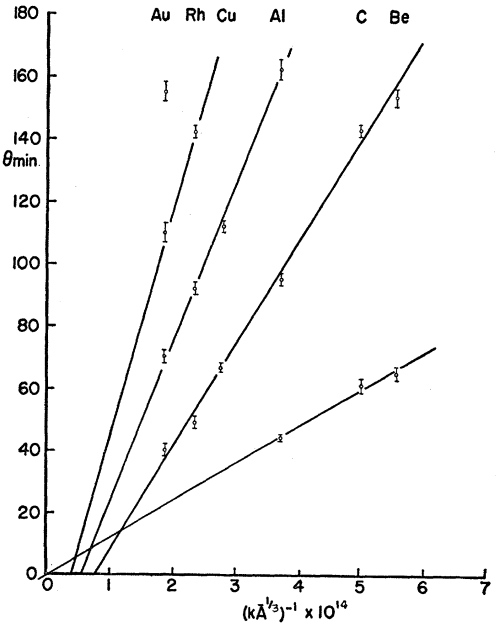

FIG. 11. Location of the minima in the scattering cross section as a function of nuclear radius.

A five-parameter optical model which includes a "fuzzy" boundary and a phenomenological spin-orbit potential of the $(1/r)(\partial V/\partial r)$ type is being used in an attempt to fit the data.[4] Recent results of the Saxon group[17] indicate that quite good fits can be obtained out to about 140° for the heavy elements using only a four-parameter optical model (without spin-orbit coupling). Although the spin-orbit term is expected to improve the fit at higher angles, recent experimental data for Ta and Bi from this laboratory[18] indicate that it may be necessary to take the shape of the nucleus into account.

[17] D. Saxon (private communication).
[18] G. Schrank, Phys. Rev. 99, 640(A) (1955).

APPENDIX[19]

Consider the scattering by a thin foil of a homogeneous, nondivergent, beam cylinder with horizontal and vertical cross-sectional symmetry, into a detector aperture also with horizontal and vertical symmetry. It is necessary to find the yield from an element of area on the target foil $(d\zeta,d\eta)$ into the element of area on the detector window (dx,dy) and then integrate over the two areas. This infinitesimal yield is

$$dY=\frac{Nn\tau}{R^2}(\cos\chi)\sigma(\theta)d\zeta d\eta dxdy,$$

where R=distance from $d\zeta d\eta$ to $dxdy$, χ=angle between R and the normal to the detector window, θ=angle between the beam filament which passes through $d\zeta d\eta$ and R, x and y are the Cartesian coordinates of the detector aperture, ζ and η are the Cartesian coordinates of the beam "shadow" on the foil, N=number of incident particles per square cm per sec, n=density of target nuclei in foil, τ=foil thickness, and $\sigma(\theta)$=differential scattering cross section in the laboratory system.

Expanding to second order and dropping linear terms because of symmetry gives

$$Y=\frac{Nn\tau\sigma(\theta_0)}{R_0^2}\int\Big\{1+3R_0^{-2}C^2\zeta^2-\tfrac{3}{2}R_0^{-2}(x^2+y^2+S^2\zeta^2+\eta^2)+\frac{\sigma'(\theta_0)}{\sigma(\theta_0)}[\tfrac{1}{2}R_0^{-2}S_0^{-1}C_0(y^2+\eta^2)+3R_0^{-2}CS\zeta^2]+\frac{\sigma''(\theta_0)}{\sigma(\theta_0)}[\tfrac{1}{2}R_0^{-2}(x^2+S^2\zeta^2)]\Big\}dxdyd\zeta d\eta,$$

where θ_0=angle between the central beam filament and R_0 (see Fig. 12), R_0=distance between the center of the beam shadow on the foil and the center point of the detector aperture, $C=\cos(\theta_0-\varphi)$, $S=\sin(\theta_0-\varphi)$, $S_0=\sin\theta_0$, and $C_0=\cos\theta_0$.

For the case where the detector aperture is rectangular with a width and height w and h respectively and the beam cylinder is of negligible cross section,

[19] It is a pleasure for one of us (G.S.) to thank Dr. Walter Aron for the tedious job of checking the algebra involved in this derivation.

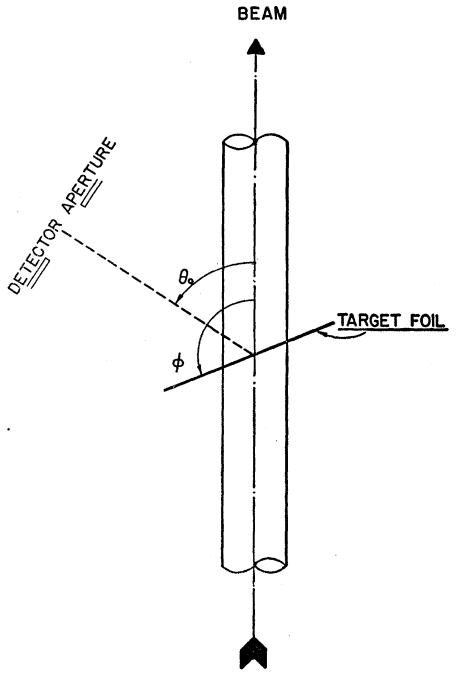

FIG. 12. Definition of angles used in the calculation of geometrical corrections.

this expression becomes

$$Y=Y_0\Big[1-\frac{w^2+h^2}{8}+\Big(\frac{h^2\cot\theta_0}{24}\Big)\frac{\sigma'(\theta_0)}{\sigma(\theta_0)}+\frac{w^2}{24}\frac{\sigma''(\theta_0)}{\sigma(\theta_0)}\Big],$$

where $y_0=(Nn\tau/R^2)\sigma(\theta_0)A_1A_2$, A_1=area of rectangular detector aperture, and A_2=area of target foil struck by the beam. Except for the second term in the bracket, this agrees with the expression used by Lyman, Hanson, and Scott.[20]

For the case where the detector aperture is circular with radius b, the beam cylinder circular in cross section with radius a, and the foil turned at an angle φ with respect to the beam axis, the result is

$$Y=Y_0\Big\{[1+\tfrac{3}{8}R_0^{-2}(\sin^{-2}\varphi)a^2(2C^2-S^2-\sin^2\varphi)-\tfrac{3}{4}R_0^{-2}b^2]+[\tfrac{1}{8}R_0^{-2}S_0^{-1}C_0(a^2+b^2)+\tfrac{3}{4}R_0^{-2}CSa^2(\sin^{-2}\varphi)]\frac{\sigma'(\theta_0)}{\sigma(\theta_0)}+[\tfrac{1}{8}R_0^{-2}(a^2S^2\sin^{-2}\varphi+b^2)]\frac{\sigma''(\theta_0)}{\sigma(\theta_0)}\Big\}.$$

[20] Lyman, Hanson, and Scott, Phys. Rev. 84, 626 (1951).